Seismic performance of historic bridge piles

Lead Investigator:

Dr. Lucas Samuel Hogan,
Civil and Environmental Engineering, University of Auckland

Research Team:

Dr. Lucas Samuel Hogan, Dr. Max Stephens,
Prof. Liam Wotherspoon, Dr. Pavan Chigullapally
Civil and Environmental Engineering, University of Auckland

June 9, 2023

Acknowledgements

The research team would like to acknowledge the financial contribution of Toka Tū Ake EQC and QuakeCoRE for supporting the experimental costs associated with this project as well as the funding for Dr. Chigullapally's PhD. The team would also like to thank Dr. Andrew Stolte, Mr. Mohamed Mostafa, Mr. Mark Byrami, Mr. Patrick Rogers, Mr. Peng Zhang for their assistance in preparing and conducting the field testing. Finally the assistance on site provided by Brian Perry Civil and Jurgens Demolition were essential for the successful completion of these tests.

Executive Summary

Approximately half of the New Zealand State Highway bridges were constructed prior to the development of any specific design for seismic loads. Recent earthquakes have shown that generally these bridges sustain only minor damage when subjected to earthquakes, however, the observable portions of these bridges are all above ground. There is still concern about the ability of the pile foundations that support these bridges to maintain stability of the bridge following an earthquake. To investigate the behaviour of these foundations, this project tested six concrete piles from the Whirokino Trestle Bridge. The Whirokino Trestle Bridge was constructed in 1939 and its pile foundations are identical to a significant number of the bridges on the State Highway system. As the Whirokino Trestle Bridge was being replaced by a new adjacent bridge, six piles were isolated and tested as part of the bridge demolition. The piles were subjected to lateral loads to simulate earthquake demands. All six piles performed similarly and were able to sustain their load capacity even when at significant lateral deformations. This testing shows that these pile foundations on the older bridges on the State Highway network are likely to perform well during an earthquake and help enable a resilient transportation network.

Technical Abstract

Approximately half of the New Zealand State Highway system was constructed before the development of seismic design criteria. While many of these bridges have performed well when subjected to inertial loads in previous earthquakes, the lightly reinforced pile foundations are a potential vulnerability of these bridges, particularly since they are utilized in a significant number of the State Highway bridge stock. Furthermore, the piles on these older bridges all utilized plain round reinforcement and as such there is limited previous studies on the likely seismic performance of these types of piles.

To investigate the performance of these piles, six piles were isolated and subjected to cyclic lateral loading from the Whirokino Trestle Bridge following its demolition. The Whirokino Trestle Bridge was constructed in 1939 and is representative of many bridges on the New Zealand State Highway Network. The piles were founded in stiff sand and were subjected to different lateral loading protocols to investigate the lateral behaviour under low level excitation, large monotonic loading as is typical in lateral spreading, and to large cyclic deformation as is typical for large ground shaking. Numerical models were also utilized to investigate subgrade behaviour of the piles as their historic nature meant that instrumentation could not be installed below grade. It was found that prior to pile yielding the foundation response was dominated by the combine soil-pile stiffness. Following yielding of the pile, the lateral response was dominated by the pile stiffness. The piles were able to sustain their nominal moment capacity to approximately 0.45 pile diameters with no drop in load or pinching of hysteresis. These tests indicate that these historic bridge piles are likely to perform well in an earthquake.

Keywords

Pile foundations; bridges; seismic; quantifying hazards and impacts;

Introduction

Many in-service reinforced concrete bridges constructed around the world in the first half of the 20th century were designed without any seismic guidelines and often utilized smooth reinforcement for the longitudinal reinforcing (Freeman, 1932; Beavers, 2002; Fajfar, 2018; Hogan et al. 2013, Lew et al., 2020). During this period, there was little in the way of seismic detailing and reinforcing requirements (Seible et al., 1995; Maffei, 1996). In New Zealand, bridges designed between 1930's to mid-1960's were only required to resist a lateral force equal to 10% of the mass of the superstructure irrespective of the location or geometry of the bridge. This lateral force was equally distributed among all the piers and its foundations based on the tributary area of the piers (Hogan et al., 2013). While these bridges were designed with limited knowledge of seismic detailing, most of the bridges of this era performed well in previous earthquakes under moderate levels of shaking, due to their short lengths and low pier heights (Lew et al., 2020). In recent earthquakes some of the bridges from this era were in areas that experienced strong levels of shaking in New Zealand, with damage observed as a result of inertial response and lateral spreading induced loading (Davies et al., 2017; Giovinazzi et al., 2011; Palermo et al., 2010, 2011, 2017; Stringer et al., 2017). As most of the damage observations following these earthquakes were related to the superstructure and the above ground sections of the substructure, there is still uncertainty regarding the expected performance of pile foundations of these bridges with older pile foundations subjected to these loading conditions.

In general, the outcomes from previous research have provided designers with improved estimates of the lateral response of pile foundations across a range of pile foundation designs and soil profile characteristics (Matlock (1970), Kramer (1991), Rollins et al. (1998), Sritharan et al. (2007)). However, even with the considerable number of large-scale pile and in service tests in the existing literature, there are few tests on piles with smooth reinforcement and light transverse reinforcement. Adding to this, in most of the in-service tests previously performed the pile-soil system remained in the linear range, with no in-service bridge foundation tests performed under large deformations that would push the piles into the inelastic range. The lateral displacement response and capacities of pile-soil system with smooth reinforcement and light transverse reinforcement under large deformations therefore remains an area of uncertainty. It is particularly important for the New Zealand State Highways system to understand the importance of this pile type as approximately half of the bridges are founded on piles with smooth reinforcement (Hogan 2014).

This report presents the results of an experimental program to assess the performance of in-service pile foundations during the demolition of the Whirokino Trestle Bridge (ca. 1939) in Foxton, New Zealand (Figure 1). A series of lateral loading tests were performed in order to characterize the response of the bridge pile foundations with smooth reinforcement. Six piles were tested and each precast reinforced concrete pile had an octagonal cross section 406 mm wide and a length of approximately 9.2 m from the base of the pile cap. The pile reinforcement consisted of eight 22 mm diameter longitudinal bars and 4 mm diameter spiral transverse reinforcement at 50 mm pitch along the length of pile (Figure 2). All reinforcement was smooth reinforcement, with a yield strength (f_y) of 288 MPa. Piles were driven into the soil profile and the top 1.0 m of the piles had the cover stripped following installation before they were cast into the pile cap during construction. Further characteristics of the Whirokino Bridge, the foundation system, and the soil profile at the testing sites are presented in Appendix A. The preparation of the test specimens during the demolition process and the test setup, including the instrumentation layout and the field-testing methodology are also presented in Appendix A. The results of each pile test are discussed individually in Appendix B and the development of the numerical model used to interrogate the field-testing results is described in Appendix C.

Figure 1: The Whirokino Trestle Bridge in Foxton, NZ prior to demolition.

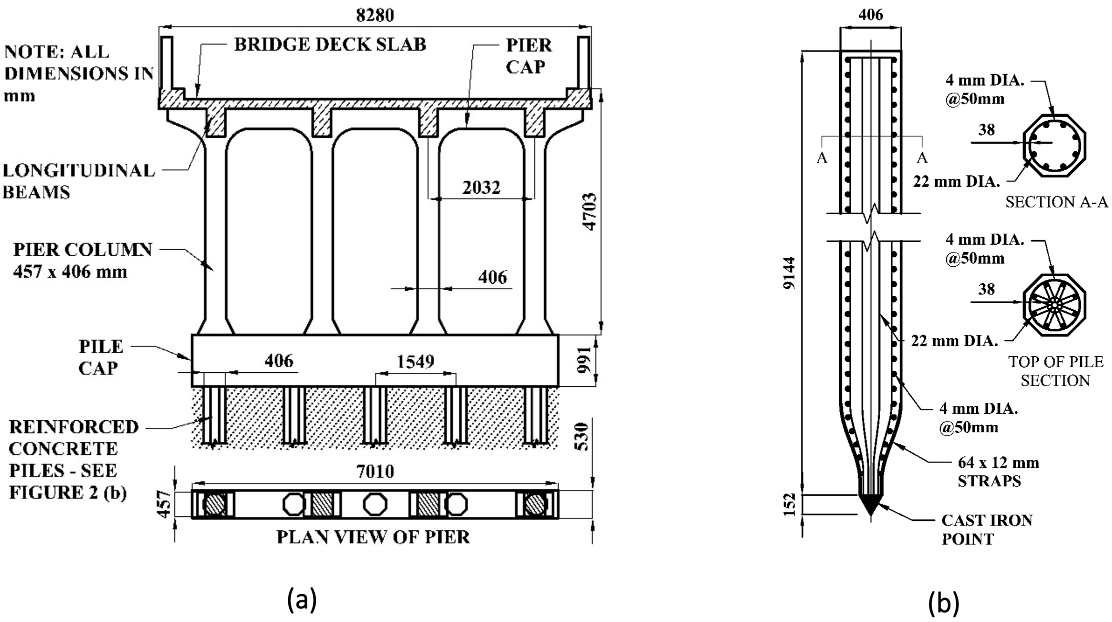

Figure 2: Whirokino Trestle Bridge (a) typical pier dimension details; (b) pile dimensions details.

Discussion

This section discusses the common trends observed across all six pile tests. The load-displacement characteristics from the tests (see Appendix A) suggests that all pile-soil systems behaved elastically until 80% of the peak load or up to a pile head displacement of 7% of pile diameter (around 30 mm). After this point, a plastic hinge developed, leading to a reduction in the stiffness of the system.

In the Pile 2, Pile 3, and Pile 5 tests, a clear yield point was observed in both the loading directions, while in the Pile 1, Pile 4 and Pile 6 tests, a clear pile-soil system yield point was observed in the north direction only. All pile-soil systems will have yielded in both the loading directions, with the absence of a clear yield point for loading in the south direction for Piles 1, 4 and 6 most likely due to the application of loading above the pile-soil system yield point in the initial loading cycle in the northern direction. A typical hysteretic response from the pile top is shown in Figure 3. Irrespective of the pile location, loading protocol and the number of load cycles a pile had experienced, the unloading path and the residual displacement in all the pile-soil systems were similar when the pile was unloaded from similar peak displacements values. The unloading and reloading stiffness of the system was slightly lower than the initial elastic stiffness of the system, likely due to the pile cross-sectional characteristics dominating the response of the system and the slight reduction in stiffness could be due to soil gapping and cracking.

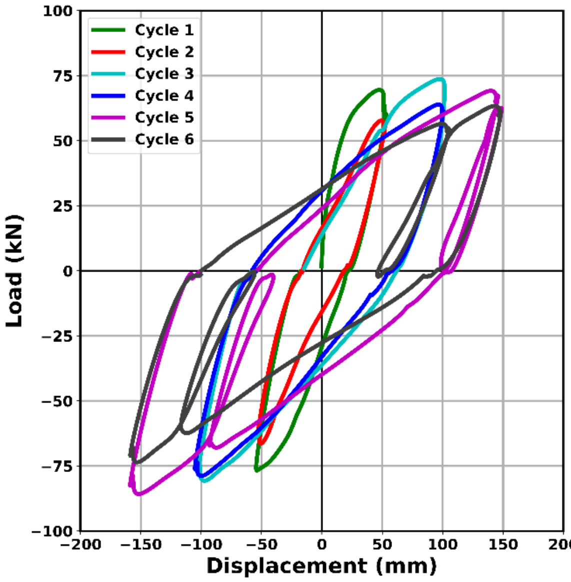

Figure 3: Load-displacement measured at the top of pile cap in Pile 6

A response similar to these pile tests has been observed in column tests with smooth reinforcement (Dekker, 1992; Di Ludovico et al., 2014; Goksu et al., 2014; Maffei, 1996), where the columns retained their strength through large displacements and multiple cycles of loading. In these column tests, during unloading of the columns, there was no lateral resistance offered by the column due to large bar slip in critical areas, causing marked pinching in the load-displacement hysteresis loops. Interestingly, there was no such pinching behaviour observed in the load-displacement hysteresis loops from these pile tests, despite the likely development of bar slip in the region of the pile experiencing the maximum bending moment, which effectively allowed the pile section to rock back and forth. The lack of pinching behaviour could be due to additional confinement provided by the surrounding soil to the cover concrete thereby limiting spalling Allotey and El Naggar (2008) showed soil confinement effects for undamaged piles can be low, but for damaged piles, the extra confinement provided to the damaged zone by the cave-in of soil (especially in sandy soils) could contribute significantly to the improvement of the pile-soil system performance. The confining pressure provided by the soil in the plastic hinge regions can significantly increase the effective confinement of the section and prevent the development of high levels of localized plastic rotation. This results in an elongated hinge region and a sizable increase in ductility capacity of the pile-soil system.

The load-displacement response from field testing and the numerical model at the top of Pile 1 are compared in Figure 4(a) along with the key points of the hysteretic response. The response of Pile 1 is indicative of the backbone response of all six test piles. In general, the numerical model of Pile 1 was able to provide a satisfactory match with the observed field-testing response in terms of peak loads, residual displacements, overall hysteretic path, and rotations at the top of pile. The global response of the pile-soil system was nominally linear through to the first yield of pile reinforcement (referred to as first yield), with the softening of the system through this range a result of soil nonlinearity and gap opening. When the nominal moment capacity was reached, there was a significant softening of the pile-soil system both in the model and field-testing results. Nominal moment capacity of the pile section was defined as the moment at which the crushing of cover concrete was initiated in the compression region. After reaching the peak load in the positive direction, the deformation of the pile-soil system increased without any strength degradation up to the target peak displacement. There was no suggestion of bar buckling based on the numerical modelling results as the tension strains in the reinforcement were within the limits prescribed by Feng et al., (2014). The piles were all able to sustain significant deformation capacity up to 0.6 pile diameters without strength degradation indicating very robust performance.

Figure 4(b) presents the variation of the bending moment profile from the Pile 1 numerical model at key points of the hysteretic response. The location of peak bending moment varied between 2.2*D* and 3*D*, (where *D*= diameter of the pile) between the cracking and first yield moments and remained at this depth until the nominal moment capacity of the pile section was reached. At this point, the location of peak bending moment had moved down to 3.5*D* and remained at this position as the applied displacement increased. This location then stayed relatively stable for the remainder of the loading cycle through to the target peak loading in the negative direction. The depth of soil gapping from the model remained relatively consistent at approximately 0.9*D* (0.35 m) below the peak bending moment depth after the nominal moment capacity in the positive loading direction had been reached. A similar gap depth opened up during loading in the negative direction, with this depth also stabilising at 0.9D below the peak bending moment depth.

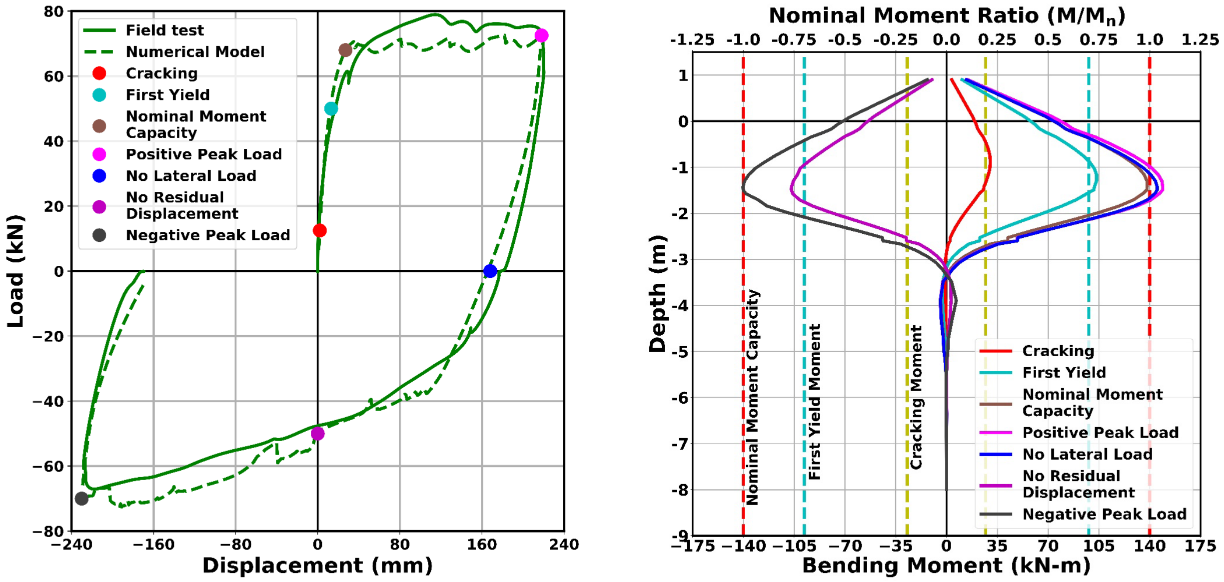

(a) (b)

Figure 4: Single cycle pushover results of Pile 1 (a) Comparison between field test and numerical model load-displacement behaviour at the top of pile cap; (b) Bending moment distribution along the depth of the pile at different load points from numerical model.

To evaluate the influence of the bond-slip material model, which accounts for the behaviour of the smooth reinforcement, on the response of the pile-soil system, the Pile 2 numerical model was analysed without a bond-slip implementation. The load-displacement response of Pile 2 numerical model with the bond-slip model is shown in Figure 5(a) and the model that does not account for bond-slip is shown in Figure 5(b). The bending moment distribution with depth for Pile 2 is shown in Figure 6 with the bond-slip version in Figure 6(a) and the model that neglects bond-slip in Figure 6(b). The secant stiffness of the model without bond-slip implementation in the first three loading cycles was 15-20% higher than the model with bond-slip. The peak loading values across all cycles were 5-10% higher compared to the model with bond-slip. Although the model without bond-slip had similar loading and unloading path shape to the model with bond-slip, the amount of energy dissipated, represented by the area inside the hysteresis loop for the model without bond-slip was around 10-20% higher than model with bond-slip. The numerical model without bond-slip was not able to capture the reduction in stiffness and flattening of the hysteretic response after reaching the system softening point even though the model had reached the nominal moment capacity in Cycle 3. The nominal moment capacity of the system without bond-slip was 25% higher and the location of peak bending moment was 0.5*D* lower, when compared to the system with bond-slip (Figure 3-12(b)). The length of the pile above the nominal moment capacity was also higher in model without bond-slip when compared to the model with bond-slip for similar pile head displacements, likely resulting from the increased stiffness of the pile.

Figure 5 suggests the global cyclic response of model without bond-slip moved further away from the response of model with bond-slip, showing that the bond-slip model implementation was able to improve the ability of the model to better capture the global cyclic response of the pile-soil system and the stiffness and strength degradation. However, this improvement was not as significant as that observed in other structural elements (like beams and columns) with smooth reinforcement. This is because the response of system and hysteretic shape for other structural elements are governed by the bond-slip behaviour in the plastic hinge regions. Even though the response of pile-soil system and its hysteretic shape is influenced by the properties of the pile in the plastic hinge regions, the presence of the soil and the resistance it provided in the pile active length regions seems to reduce the influence of bond-slip. This was evidenced by the non-pinched hysteretic response observed despite curvatures from the field testing and numerical models exceeding the limits proposed by the Dhakal and Fenwick (2008) and that observed during the laboratory testing of Whirokino Trestle Bridge columns with smooth reinforcement by Dekker (1992) and Maffei (1996).

The sensitivity of the model to the bond-slip model implementation was further explored by varying the length of pile over which the model was applied. The extent of bond-slip was determined using the recommendations of CEB-FIP (2000). The influence of extent of bond-slip model implementation on the response of pile-soil system was studied by implementing the bond-slip material model only in the regions of bond-slip occurrence (1 m above and below the location of maximum moment, which is 0.5 m to 2.5 m below the ground level), and by implementing the original bilinear steel reinforcement material model along the rest of the pile length. The response of this pile-soil system was similar to the response of Pile 2 model with bond-slip implementation, suggesting that the implementation of the bond-slip model in the regions of bond-slip occurrence will be able to capture the global cyclic response.

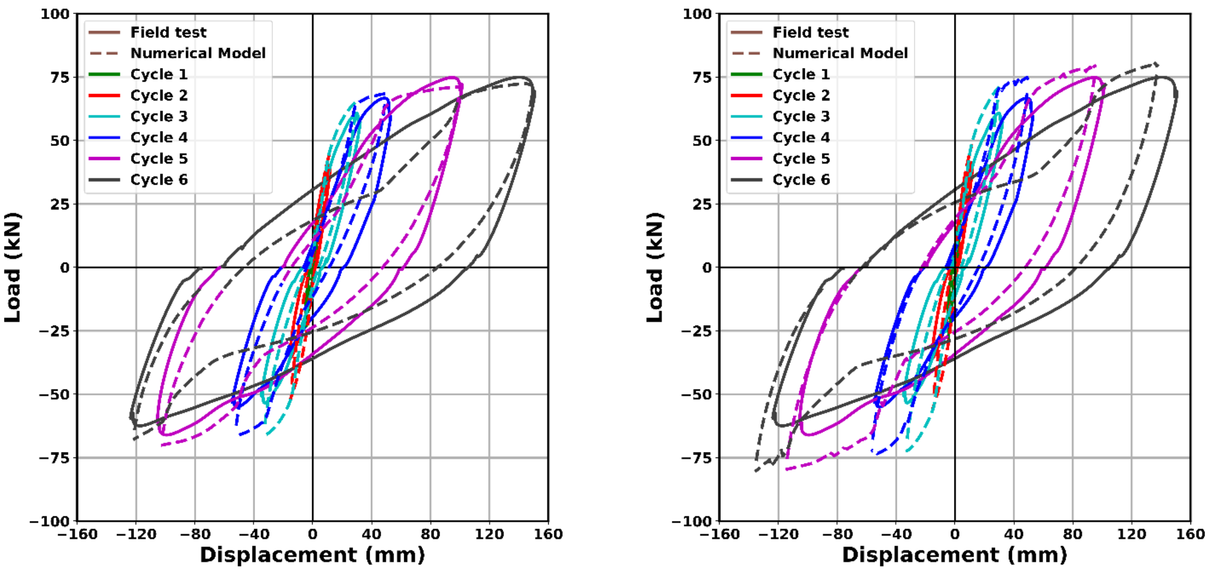

(a) (b)

Figure 5: Comparison between field test (solid lines) and numerical model (dashed lines) load-displacement behaviour at the top of pile cap under increasing cyclic pushover results of Pile 2 (a) with bond-slip; (b) without bond-slip.

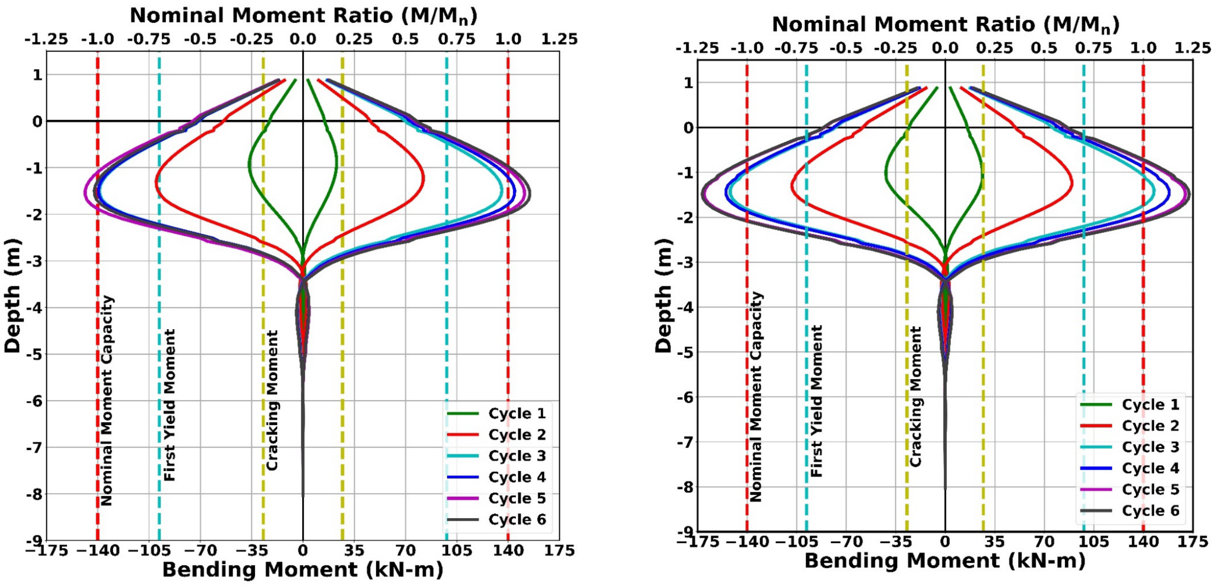

(a) (b)

Figure 6: Comparison of bending moment distribution along the depth of the pile at different load points under increasing cyclic pushover results of Pile 2 numerical model (a) with bond-slip; (b) without bond-slip.

To investigate trends in pile performance, several normalised criteria were investigated for all six piles. The variation of average cycle stiffness with normalised average peak cycle displacement (NAPCD) at top of pile cap is presented in Figure 7. NAPCD for a cycle was defined as the average of the peak displacement reached in the positive and negative loading direction for a given cycle divided by the pile diameter. Due to the high initial loading in the first cycle in Pile 3 and Pile 6, their initial cycle stiffness was around 60% and 70% of the initial cycle stiffness of Pile 2 and Pile 5. The stiffness of the pile-soil system degraded rapidly in the lower NAPCD range (below 0.07), where the stiffness contribution to the system was from both soil and pile. This stiffness degradation was due to the plastic deformation of the soil, along with degradation of pile stiffness due to cracking in this load range. At higher NAPCD (above 0.07), the rate of stiffness degradation reduces. At this point, the stiffness of pile dominates the system stiffness and the degradation of pile stiffness only contributes to the pile-soil stiffness degradation in this load range. Irrespective of the soil profile and loading protocol, the relationship between average cycle stiffness with NAPCD was similar across all tests. This indicates that the pile properties are dominating the response of the pile-soil system, with little influence from the variability in the soil profile characteristics.

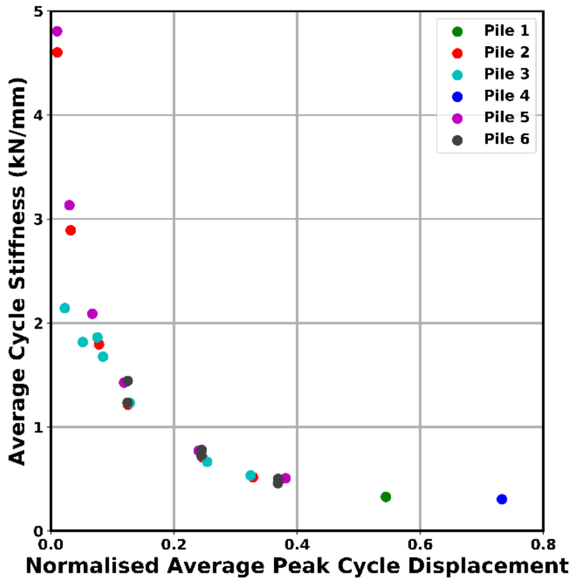

Figure 7: Variation of average cycle stiffness with normalised average peak cycle displacement at the top of pile cap.

The variation of normalised residual displacement at the ground level and residual rotations with respect to the normalised peak displacement at the ground level is summarised in Figure 8. Normalised residual displacement is the residual displacement in each direction of a load cycle divided by the pile diameter, and normalised peak displacement is the peak displacement in each direction of a load cycle divided by the pile diameter. Below the yield point (a normalised peak displacement of approximately 0.035) no clear residual displacement or rotations developed, with the system returning back to a similar location after each loading cycle. In this range soil nonlinearity and gapping dominated the response, with the effects in each loading direction cancelling each other out and preventing residual displacements and rotations from developing. Above the yield point there was an abrupt increase in the normalised residual displacements at ground level and residual rotations, with both demonstrating a linear relationship to the normalised peak displacements at ground level. The high normalised residual displacements and residual rotations post-yield point could be due to the incomplete closure of flexural cracks in the pile resulting from low axial load and elongation of the longitudinal reinforcement in the pile, as the response of the pile dominates the response of the system at the higher loading levels. Irrespective of the soil profile and loading protocol, the relationship between the normalised residual displacement, residual rotations and normalised peak displacement was similar across all tests.

The variation of equivalent viscous damping of a cycle with NAPCD at the top of pile cap is presented in Figure 9. The equivalent viscous damping for each half cycle of the load-displacement hysteretic loop was estimated separately by calculating the area of each half loop and considering the corresponding peak displacement and forces based on the recommendations of Priestley (2007). The average of both the half cycles was considered as the equivalent viscous damping of the overall cycle. Across all piles there was a similar trend in the relationship between equivalent viscous damping and the NAPCD. The equivalent viscous damping varied between 5-8 % before the pile-soil system yielded (NAPCD below 0.07). In this range, the equivalent viscous damping was controlled by the nonlinear response of the soil surrounding the pile. The equivalent viscous damping varied between 7-18% beyond the yield point (NAPCD above 0.07), with equivalent viscous damping significantly higher than those prior to the yield point. At these higher loading levels equivalent viscous damping was likely dominated by plastic hinge development and bar slipping in the critical areas within the pile, and as a gap had already developed on both sides of the pile, the soil would have a smaller contribution to the equivalent viscous damping. As Pile 3 was tested using an initial pre-yield load cycle followed by increasing cyclic loading, the equivalent viscous damping of the system reduced from an equivalent viscous damping value of ~7% in the high initial loading cycle to a value of ~5% in the three subsequent cycles where the load was equal to or less than that applied in the first cycle. This could be due to lack of additional soil gapping and crack formation in the pile-soil system after the high initial loading cycle, with the equivalent viscous damping increasing only increasing after the load in the initial cycle had been exceeded. The variation of equivalent viscous damping with NAPCD was similar to Priestley`s (2007) recommendations for the damping variation in a pinned head pile in sand.

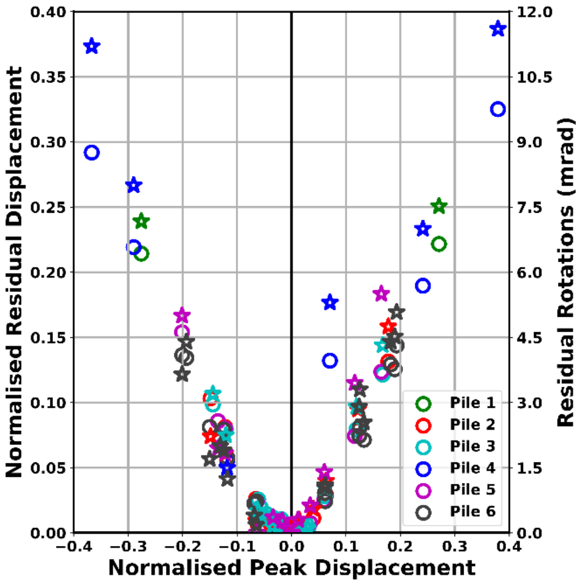

Figure 8: Variation of normalised residual displacement at the ground level (circle) and residual rotations (star) with normalised peak displacement at the ground level.

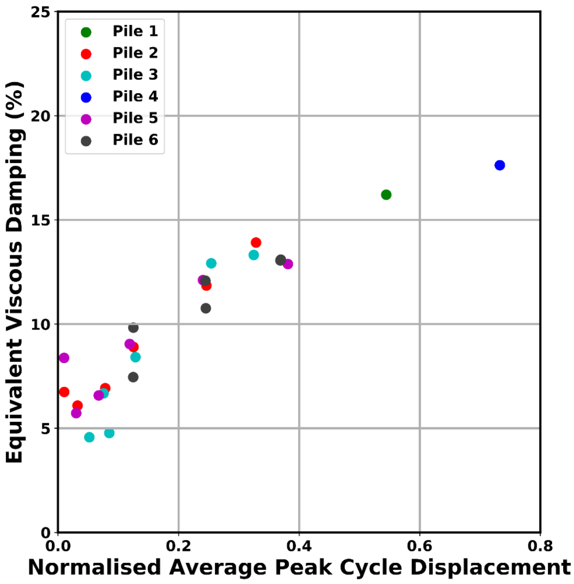

Figure 9: Variation of equivalent viscous damping of a cycle with normalised average peak cycle displacement at the top of pile cap.

Overall, the piles showed very good performance on a number of metrics. While only individual piles were tested, these piles are incorporated in pile groups at bridges piers on the State Highway network. For an integrated pile group with a pile cap beam, the response of the pile group will be different in the direction along the width of the pile cap beam and in the direction perpendicular to the pile cap beam width. In the direction along the width of the pile cap beam, the deflection capacity of the pile group would be much lower while the lateral load capacity of the pile group per pile will be higher than the isolated single pile due to the additional rotational restraint provided by the pile cap beam. In the direction perpendicular to the pile cap beam width, the deflection and lateral load capacity of the pile group per pile will be similar to that of isolated single pile due to the formation of a single plastic hinge. In addition to the above, if the pile cap is embedded into the soil, the deflection and lateral load capacity of the pile group will be increased in both the directions as the contact area is increased.

Conclusions

Cyclic pushover tests were performed on a total of six isolated piles at two test locations of the Whirokino Trestle Bridge to determine the behaviour of the isolated piles with smooth reinforcement in sandy soils. The test site and loading protocols were chosen in order to capture the response of piles under different loading conditions and to study the effects of variation in stiffness due to soil nonlinearity, gapping, cracking and yielding of the pile. Based on the field testing results, the following conclusions can be drawn:

- The pile-soil systems likely behaved elastically up to 80% of the peak load and a displacement equal to 7% of the pile diameter. At this load level the pile-soil system response was controlled by the response of the soil and was sensitive to loading protocol with a reduction of 60-70% in initial cycle stiffness depending on the intensity of initial loading applied.

- Beyond yield, the pile-soil system response was governed by the structural properties of the pile with similar cyclic stiffness, energy dissipation, and residual displacement regardless of loading protocol or soil properties.

- The pile-soil systems were able to maintain strength through large displacements and multiple cycles without any pinching in their hysteretic response. This behaviour is attributed to the confining effect of the soil surrounding the pile, preventing spalling of the cover concrete and bar buckling.

- Despite of being designed with no explicit seismic detailing, the field testing suggests that these older pile foundations are expected to have sufficient strength and deformation capacity in the event of an earthquake.

The results from the pile tests performed at the Whirokino Trestle Bridge under different loading protocols were used to validate the numerical modelling approach to replicate the response of the pile with smooth reinforcement using OpenSeesPy. The models developed account for the nonlinear soil response, pile material nonlinearities, and the bond-slip effects at the interface between the smooth reinforcing and surrounding concrete. Based on the numerical modelling results comparison with field test results and sensitivity studies performed on the key parameters controlling the response of the pile, the following conclusions can be drawn:

- The procedures developed to model the stress-strain response of smooth reinforcement accounting for reinforcement bond-slip were successful in replicating the response of the piles with smooth reinforcement.

- The global response of the pile-soil system with smooth reinforcement in numerical models was fairly linear until the system reached the nominal capacity, after which significant softening of the system was observed. These pile-soil systems were able to maintain their strength through large displacements and multiple cycles without any pinching in their hysteretic response due to the confining effect of the soil surrounding the pile, preventing spalling of the cover concrete and bar buckling.

- Incorporating reinforcing bond-slip into the model enabled it to better capture the global cyclic response of the pile-soil system and the influence of repeated loading cycles on the stiffness and strength degradation. There was around 10% variation across different metrics when bond-slip was not considered.

Future Work

Following on from the testing of the bridge piles of the Whirokino Trestle Bridge, the research team was able to leverage this EQC Toka Tū Ake funding to secure QuakeCoRE funds for the extraction and testing of three bridge piers from the Whirokino Trestle Bridge. Like the tested piles, these bridge piers are representative of many other bridges on the State Highway network and were designed without any specific seismic design or detailing. The three bridge piers each suffered corrosion damage, with a mildly damaged pier, moderately damaged, and heavily damaged bridge pier extracted. This work will help inform Waka Kotahi NZTA about the seismic vulnerability of this bridge type and help with decision making about remediation and replacement time frames. These tests are currently underway at the University of Auckland (see Figure 10) and will be concluded by the end of 2023.

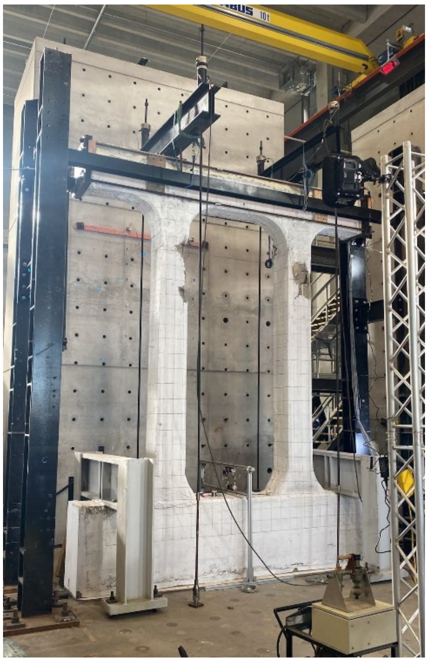

Figure 10: Extracted bridge pier test set up

Publications and Communications

Chigullapally, P., Hogan, L.S., Wotherspoon, L., (2021) Monotonic and Cyclic Pushover Testing of Isolated Piles of the Whirokino Trestle. NZSEE Annual Conference

Norman, C. (2020) Almost 100-year-old Horowhenua bridge put through its paces in earthquake test. October 6, 2020. 1 News

Karauria, M. (2020) Cutting-edge research on Whirokino Bridge - the envy of international engineers and scientists. June 3, 2020. New Zealand Herald

Karauria, M. (2020) Research on bridge 'unique'. Work on 90-year-old structure offering invaluable insights, say uni academics. June 5, 2020. Horowhenua Chronicle

Karauria, M. (2020) Old bridge reveals quake secrets. June 11, 2020. Manawatu Chronicle

Moore, R., (2020). Seismic research starts on Foxton's Whirokino Trestlebridge site. (May 12, 2020) Stuff.co.nzhttps://www.stuff.co.nz/national/300009988/seismic-research-starts-on-foxtons-whirokino-trestle-bridge-site

References

Allotey, N., & El Naggar, M. H. (2008a). A numerical study into lateral cyclic nonlinear soil–pile response. *Canadian Geotechnical Journal*, *45*(9), 1268–1281.

Andriono, T., & Park, R. (1986). Seismic Design Considerations of the Properties of New Zealand Manufactured Steel Reinforcing Bars. *Bulletin of the New Zealand National Society for Earthquake Engineering*, *19*(3), 213–246. https://doi.org/10.5459/bnzsee.19.3.213-246

Beavers, J. E. (2002). A review of seismic hazard description in US design codes and procedures. *Progress in Structural Engineering and Materials*, *4*(1), 46–63. https://doi.org/10.1002/pse.106

Boulanger, R. W., Curras, C. J., Kutter, B. L., Wilson, D. W., & Abghari, A. (1999). Seismic soil-pile-structure interaction experiments and analyses. *Journal of Geotechnical and Geoenvironmental Engineering*, *125*(9), 750–759.

Davies, T. G., & Budhu, M. (1986). Non-linear analysis of laterally loaded piles in heavily overconsolidated clays. *Géotechnique*, *36*(4), 527–538.

Davies, A. J., Sadashiva, V., Aghababaei, M., Barnhill, D., Costello, S. B., Fanslow, B., … Wotherspoon, L. M. (2017). Transport infrastructure performance and management in the South Island of New Zealand, during the first 100 days following the 2016 Mw 7.8 "Kaikōura" earthquake. *Bulletin of the New Zealand Society for Earthquake Engineering*. https://doi.org/10.5459/bnzsee.50.2.271-299

Dehestani, M., & Mousavi, S. S. (2015). Modified steel bar model incorporating bond-slip effects for embedded element method. *Construction and Building Materials*, *81*, 284–290. https://doi.org/10.1016/j.conbuildmat.2015.02.027

Dekker, D. R. (1992). *The Repair and Strengthening of Reinforced Concrete Bridge Piers*. University of Canterbury.

Dhakal, R. P., & Fenwick, R. C. (2008). Detailing of plastic hinges in seismic design of concrete structures. *ACI Structural Journal*, *105*(6), 740–749. https://doi.org/10.14359/20102

Di Ludovico, M., Verderame, G. M., Prota, A., Manfredi, G., & Cosenza, E. (2014). Cyclic Behavior of Nonconforming Full-Scale RC Columns. *Journal of Structural Engineering*, *140*(5), 04013107. https://doi.org/10.1061/(asce)st.1943-541x.0000891

Evangelio, C. D. L. (2021). *Fragility Models for Wall-type Pier Bridges in New Zealand*. The University of Auckland.

Fajfar, P. (2018). Analysis in seismic provisions for buildings: past, present and future. *Bulletin of Earthquake Engineering*, *16*(7), 2567–2608. https://doi.org/10.1007/s10518-017-0290-8

Feng, Y., Kowalsky, M. J., & Nau, J. M. (2014). Deformation limit states for longitudinal bar buckling in RC circular columns considering the effect of seismic load history. In *NCEE 2014 - 10th U.S. National Conference on Earthquake Engineering: Frontiers of Earthquake Engineering*. https://doi.org/10.4231/D3TX35675

Freeman, J. R. (1932). *Earthquake Damage and Earthquake Insurance*. New York: McGraw-Hill Book Company.

Goksu, C., Yilmaz, H., Chowdhury, S. R., Orakcal, K., & Ilki, A. (2014). The effect of lap splice length on the cyclic lateral load behavior of RC members with low-strength concrete and plain bars. *Advances in Structural Engineering*, *17*(5), 639–658. https://doi.org/10.1260/1369-4332.17.5.639

Giovinazzi, S., Wilson, T., Davis, C., Bristow, D., Gallagher, M., Schofield, A., … Tang, A. (2011). Lifelines performance and management following the 22 February 2011 Christchurch earthquake, New Zealand: Highlights of resilience. *Bulletin of the New Zealand Society for Earthquake Engineering*, *44*(4), 402–417. https://doi.org/10.5459/bnzsee.44.4.402-417

Hogan, L. S., Wotherspoon, L. M., & Ingham, J. M. (2013). Development of New Zealand seismic bridge standards. *Bulletin of the New Zealand Society for Earthquake Engineering*.

Hogan, Lucas S. (2014). *Seismic Response Categorisation of New Zealand Bridges*. Standards New Zealand.

Kramer, S. L. (1991). *Behavior of piles in full-scale, field lateral loading tests*. Seattle.

Lew, S. W., Wotherspoon, L., Hogan, L., Al-Ani, M., Chigullapally, P., & Sadashiva, V. (2020). Assessment of the historic seismic performance of the New Zealand highway bridge stock. *Structure and Infrastructure Engineering*, 1–13. https://doi.org/10.1080/15732479.2020.1762675

Maffei, J. (1996). *The Seismic Evaluation and Retrofitting of Bridges*. University of Canterbury.

Mander, J. B., Priestley, M. J., & Park, R. (1988). Theoretical stress-strain model for confined concrete. *Journal of Structural Engineering*, *114*(8), 1804–1826.

Matlock, H. (1970). Correlations for design of laterally loaded piles in soft clay. *Offshore Technology in Civil Engineering's Hall of Fame Papers from the Early Years*.

Palermo, A., Heux, M. Le, Bruneau, M., Anagnostopoulou, M., Wotherspoon, L., & Hogan, L. (2010). Preliminary findings on performance of bridges in the 2010 darfield earthquake. *Bulletin of the New Zealand Society for Earthquake Engineering*, *43*(4), 412–420. https://doi.org/10.5459/bnzsee.43.4.412-420

Palermo, A., Liu, R., Rais, A., McHaffie, B., Andisheh, K., Pampanin, S., … Wotherspoon, L. (2017). Performance of road bridges during the 14 November 2016 Kaikōura earthquake. *Bulletin of the New Zealand Society for Earthquake Engineering*, *50*(2), 253–270. https://doi.org/10.5459/bnzsee.50.2.253-270

Palermo, A., Wotherspoon, L., Wood, J., Chapman, H., Scott, A., Hogan, L., … Chouw, N. (2011). Lessons learnt from 2011 Christchurch earthquakes: Analysis and assessment of bridges. *Bulletin of the New Zealand Society for Earthquake Engineering*, *44*(4), 319–333. https://doi.org/10.5459/bnzsee.44.4.319-333

Robertson, P. K. and Cabal, K. L. (2010). Guide to Cone Penetration Testing for Geotechincal Engineering.

Rollins, K. M., Peterson, K. T., & Weaver, T. J. (1998). Lateral load behavior of full-scale pile group in clay. *Journal of Geotechnical and Geoenvironmental Engineering*, *124*(6), 468–478.

Seible, F., Priestley, M. J. N., Hegemier, G. A., & Innamorato, D. (1997). Seismic Retrofit of RC Columns with

Continuous Carbon Fiber Jackets. *Journal of Composites for Construction*, *1*(2), 52–62. https://doi.org/10.1061/(asce)1090-0268(1997)1:2(52)

Sritharan, S., Suleiman, M. T., & White, D. J. (2007). Effects of seasonal freezing on bridge column–foundation–soil interaction and their implications. *Earthquake Spectra, 23*(1), 199–222.

Standards New Zealand. (2006). *NZS 3101:2006 Concrete Structures Standard*.

Stringer, M. E., Bastin, S., McGann, C. R., Cappellaro, C., El Kortbawi, M., McMahon, R., … Ntritsos, N. (2017). Geotechnical aspects of the 2016 Kaikōura earthquake on the South Island of New Zealand. *Bulletin of the New Zealand Society for Earthquake Engineering*, *50*(2), 117–141. https://doi.org/10.5459/bnzsee.50.2.117-141

Zhu, M., McKenna, F., & Scott, M. H. (2018). OpenSeesPy: Python library for the OpenSees finite element framework. *SoftwareX*, *7*, 6–11.

Appendix A Experimental Set Up

The current field testing program to isolate and test a number of piles was carried out during the demolition of the Whirokino Trestle Bridge. In the sections that follow, the characteristics of the bridge and the geotechnical site characterisation are first presented, followed by a description of the test setup, instrumentation setup, and the field-testing methodology.

Whirokino Trestle Bridge Overview

The reinforced concrete bridge had an overall length of 1.2 km and width of 8.3 m, with 90 spans that supported two lanes of traffic. A typical span is 12.2 m long and approximately 5.7 m tall. As seen in Figure A1, and Figure A2, the superstructure was supported by piers consisting of four rectangular reinforced concrete columns of 457 mm x 406 mm with a centre to centre spacing of 1.63 m, connected to a 406 mm x 558 mm pier cap. The column reinforcement consisted of four 28 mm diameter longitudinal bars and 12 mm diameter transverse reinforcement at 152 mm spacing. The column and pile cap intersection consisted of 20 mm diameter inclined long reinforcement bars (Figure A1). All the pier columns were connected to a 533 mm x 990 mm pile cap at the bottom of the pier and were supported by five precast reinforced concrete piles. The pile cap reinforcement consisted of three layers of 25 mm diameter longitudinal bars and 12 mm diameter transverse reinforcement at 254 mm spacing (Figure A1). Smooth reinforcement was used for all reinforcement in the construction of the bridge. A preliminary assessment of the bridge pier with pile foundations (Figure A1) showed that plastic hinging was expected to first occur in the piles. Therefore, it was important to study the piles under large demands in order to understand their response in the post-yield range.

Pile Foundation Characteristics and Preparation

Each precast reinforced concrete pile had an octagonal cross section 406 mm wide and a length of approximately 9.2 m from the base of the pile cap. The pile reinforcement consisted of eight 22 mm diameter longitudinal bars and 4 mm diameter spiral transverse reinforcement at 50 mm pitch along the length of pile (Figure A2). All reinforcement was smooth reinforcement, with a yield strength (fy) of 288 MPa. Piles were driven into the soil profile and the top 1.0 m of the piles had the cover stripped following installation before they were cast into the pile cap during construction.

The pile testing location was determined using the soil profile along the length of the bridge. The initial soil profile along the length of the bridge was based on a set of cone penetration tests (CPT) and rotary boreholes with Standard Penetration tests (SPT) that were conducted previously. The soil profile comprised of an upper layer of peat and the thickness of this layer gradually increased from north to south of the bridge, as shown in Figure A3. The pile testing location was chosen in the northern region of the bridge due to the thinner upper peat layer and better accessibility to the site. For precise soil profiles at test locations, four CPTs and two seismic CPTs were conducted within few metres from the test piles. Five piers from Pier 80 to Pier 76 were chosen for the field-testing program at the Whirokino Bridge (Figure A3 and Figure A4). The three middle piles from both Pier 77 and Pier 79 were isolated and selected for testing, with Piers 80, 78 and 76 left intact and used as reaction pile groups during testing. To prepare the site for testing, the bridge superstructure was first demolished down to the top of each pile cap. The soil around the test pile groups was excavated to remove soft surface soil layers and to expose the top of each pile, removing any interaction effects between the pile cap and the surrounding soil. Each test pile was isolated from the other piles in the pile group by saw cutting between each pile, creating a clear gap of 0.4 m between piles. The test piles after the demolition of the superstructure and saw cutting can be seen in Figure A5. The eastern piles of Pier 77 and Pier 79 were labelled as Pile 1 and Pile 4, the middle piles were labelled as Pile 2 and Pile 5, and the western piles were labelled as Pile 3 and Pile 6.

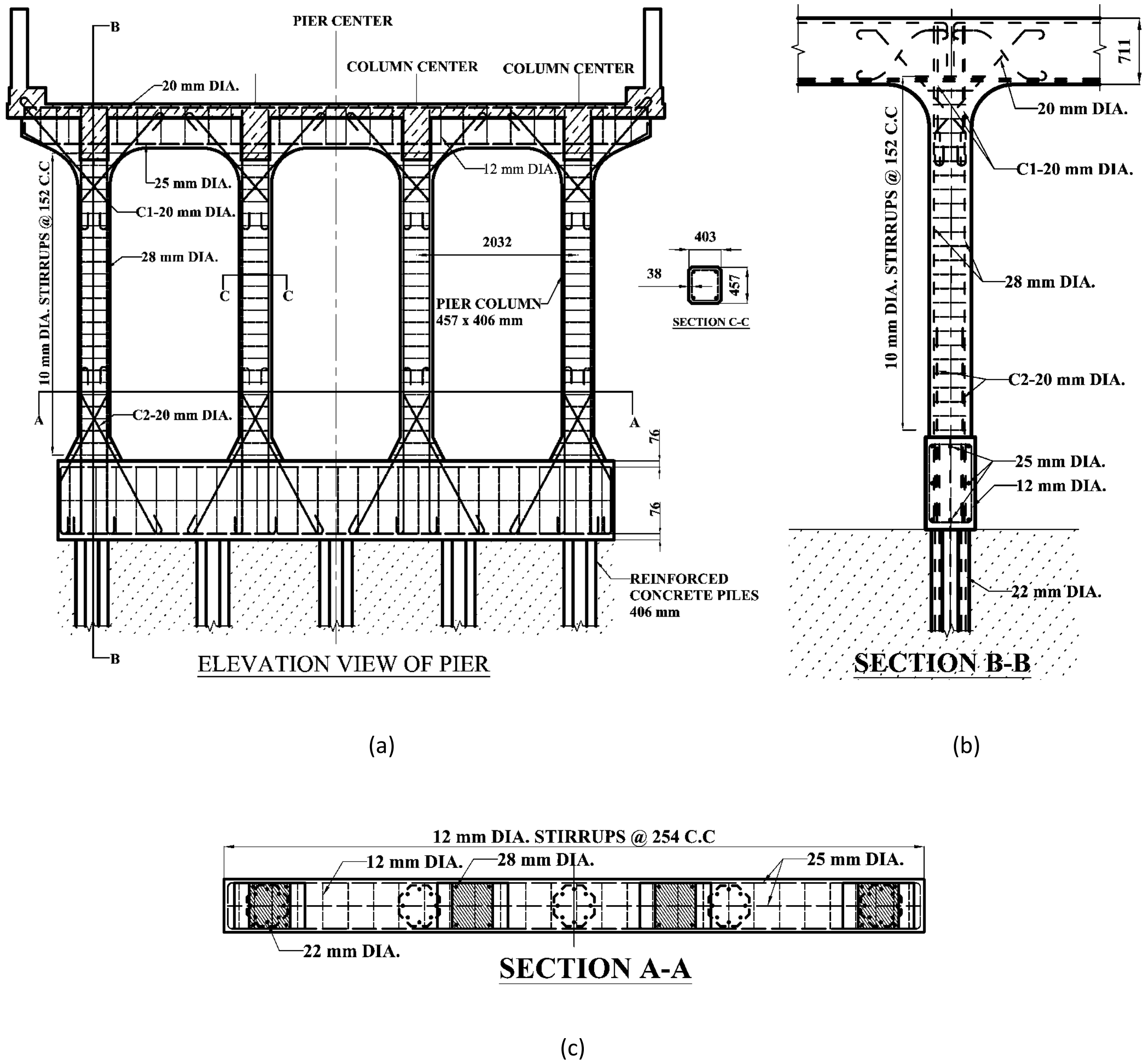

Figure A1: Reinforcement details of the Whirokino Trestle Bridge along with its foundations (a) elevation view; (b) side view; (c) plan view of a typical pier.

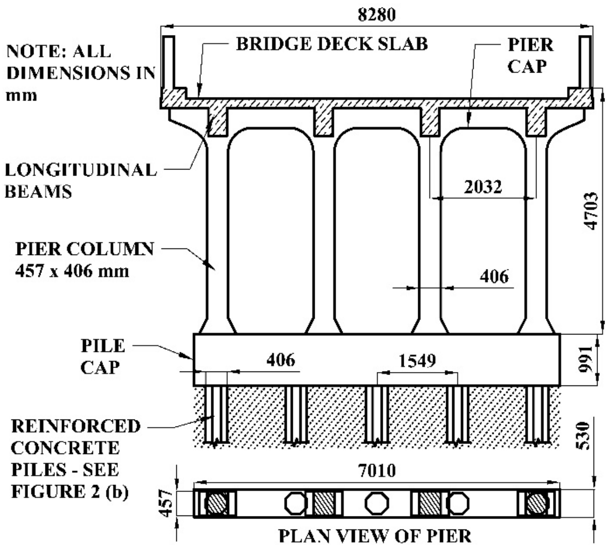

(a)

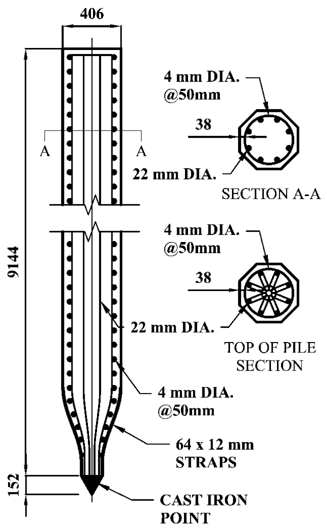

(b)

Figure A2: Whirokino Trestle Bridge (a) typical pier dimension details; (b) pile dimensions details.

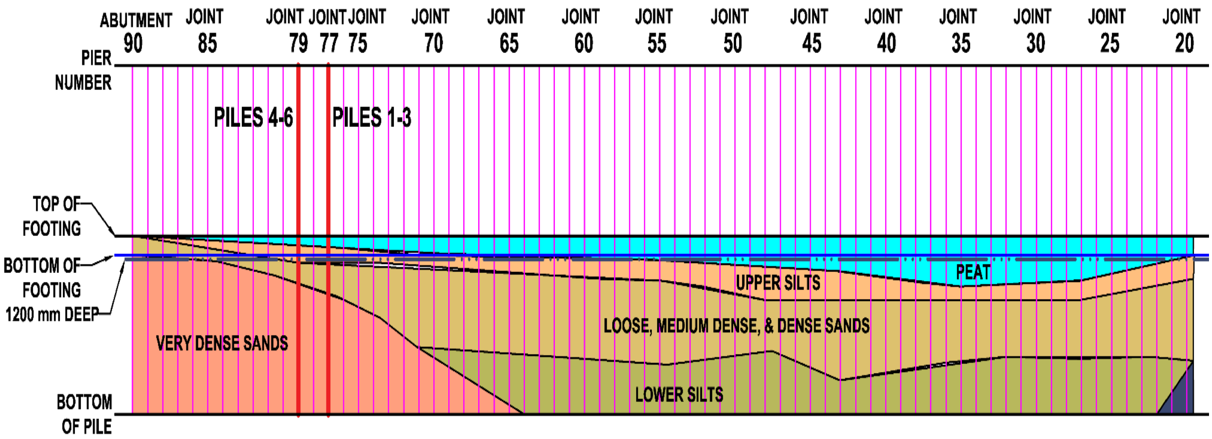

Figure A3: Variation of the soil profile along the length and depth of the Whirokino Trestle Bridge.

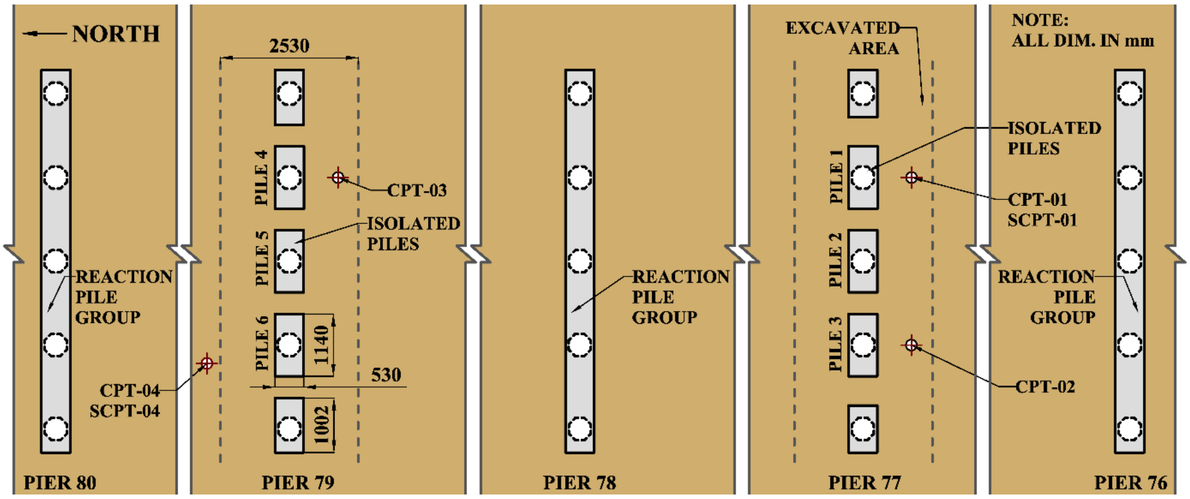

Figure A4: Plan view of test site showing locations of the test piles, reaction pile groups and geotechnical investigation locations.

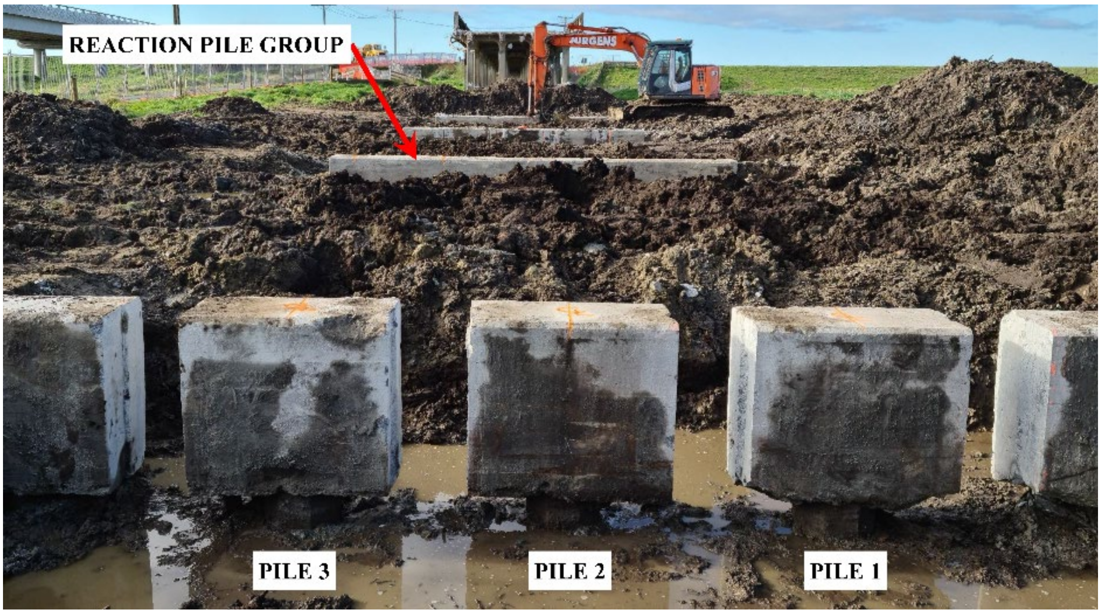

Figure A5: Test piles after isolation from the pile group and reaction pile group at test site.

Geotechnical Site Characterisation

Four cone penetrometer test (CPT) soundings and two seismic CPT (sCPT) soundings were conducted within a few metres of the test piles at the locations shown in Figure A4. The CPT tip resistance (qc), shear wave velocity (Vs) and soil behaviour type index (Ic) at both piers are summarised in Figure A6 and Figure A7. The zero depth level in these figures was around 200 mm below the bottom of pile cap for a typical test pile. At both Pier 77 and Pier 79, silty sand to sandy silt were present from the ground level to a depth of 2 m. The silty sand to sandy silt was relatively soft with an average tip resistance of 2-5 MPa and a maximum shear wave velocity between 100-135 m/s. Below this depth the soil profile transitioned to clean sands that likely extended to the base of the pile based on other investigations in the vicinity of the test area. The tip resistance rapidly increased in the clean sand layer to 25-30 MPa and the maximum shear wave velocity increased to 165-175 m/s at a depth of 4 m. The lower stratum that forms the bearing layer for the pile had a tip resistance of above 32 MPa, transitioning into very dense sands with CPT refusal.

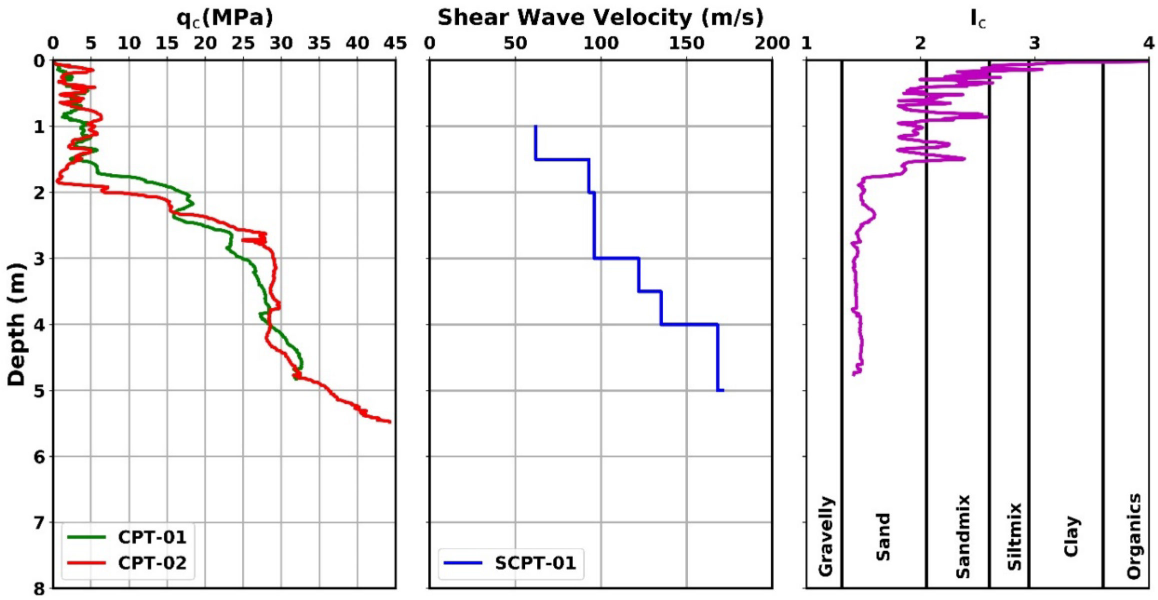

Figure A6: Geotechnical site investigation data at Pier 77: (a) Cone tip resistance profile; (b) Shear wave velocity profile; (c) Soil behaviour type index.

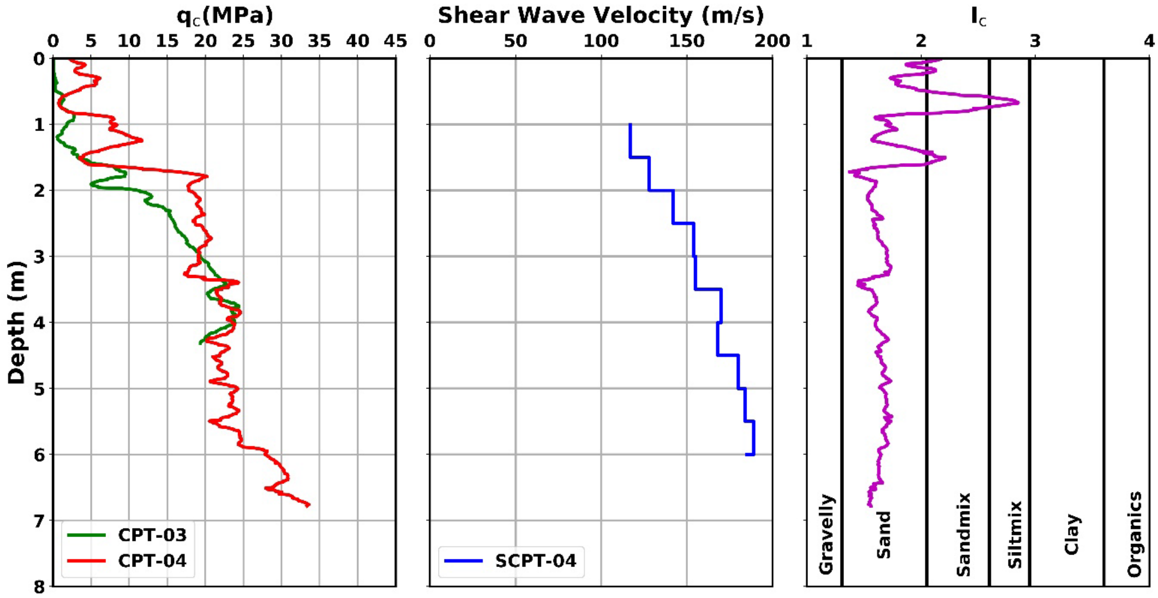

Figure A7: Geotechnical site investigation data at Pier 79: (a) Cone tip resistance profile; (b) Shear wave velocity profile; (c) Soil behaviour type index.

Test Setup

The setup used to test each isolated test pile is presented in Figure A8. To load a test pile, the adjacent pile groups were used as reaction pile groups. Piles 1-3 at Pier 77 were tested using Pier 76 and 78 as reaction pile groups, while piles 4-6 at Pier 79 were tested using Pier 78 and 80. A steel loading frame was secured with post-installed anchors at the top of the test pile and reaction pile groups. Two 19 mm wire ropes were then attached between the steel loading frames at the test pile and reaction pile groups.

To apply lateral loads to the test piles a hydraulic jack with 30 ton capacity and 300 mm stroke was placed inside the steel frame at the reaction pile group and pushed a sliding block between the steel loading frames to tension the wire ropes as can be seen in Figure A8. Through this setup, the load was applied to each test pile by pulling them towards the reaction pile group using the wire ropes. The loading was always first applied in the northern direction. The hydraulic jack was then extended to start the testing and applied until the target load or displacement was reached. The cycles with larger displacements required the wire ropes to be detached and reattached multiple times to reset the stroke of the hydraulic jacks and increase the displacement. Once each target load or displacement was reached, the wire ropes were then detached from the reaction pile group and attached the reaction pile group on the other side of the test pile to continue the loading in the opposite direction. The wire ropes were attached and detached at the reaction pile group locations in order to minimise any disturbance of the soil adjacent to each test pile. Prior to the start of every test and test setup installation, the test pits were dewatered down to the ground surface. The soil profile was therefore saturated to the ground surface at all test piles during the entire testing process.

Prior to demolition, the in-service axial load ratio on each pile due to the dead load of the bridge was less than 3.5%. As this axial load ratio was low, and due to the difficulty involved in applying additional axial load to the top of the test pile in the field, there was no axial load applied during the testing.

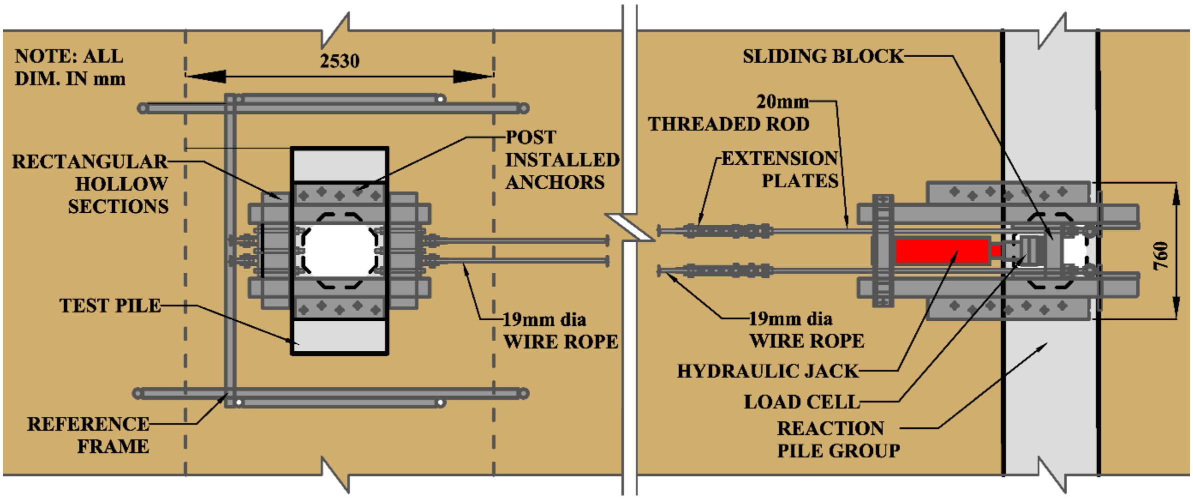

(a)

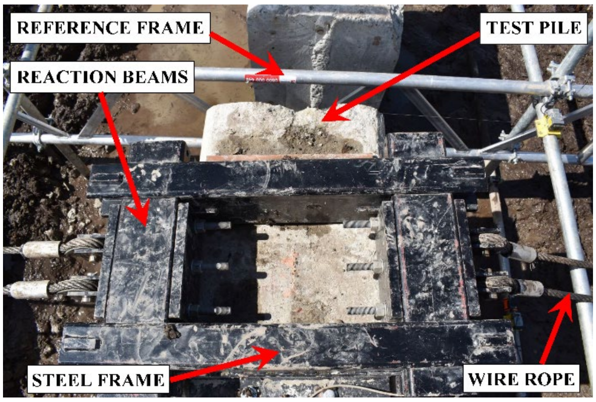

(b)

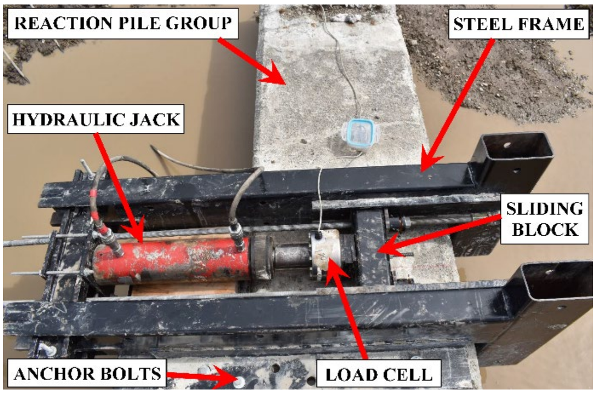

(c)

Figure A8: Summary of test setup details: (a) plan view at test pile and right reaction pile; (b) top view at test pile; (c) top view at right reaction pile.

Instrumentation

The instrumentation layout used during testing is summarised in Figure A9. Displacements were recorded using two draw-wires positioned at the top of the test pile, and one draw-wire positioned at the bottom of the test pile just above the ground surface. All the draw-wires were attached to a rigid reference frame that was embedded in the surrounding soil outside the zone influenced by soil movement during the testing (shown in Figure A8a). A unidirectional accelerometer was installed near the ground surface on each side of the pile to capture the pile rotation at this location. The distance between the top of the pile cap and the ground level varied between test specimens between 1080 mm and 1200 mm. A 25-tonne load cell was connected to the hydraulic jacks inside each loading frame to measure the applied load.

PILE	D1	D2
PILE 1	1200	1140
PILE 2	1200	1090
PILE 3	1170	1100
PILE 4	1100	1040
PILE 5	1080	1040
PILE 6	1080	1030

NOTE:
ALL DIMENSIONS IN mm
DW - DRAW WIRE
ACC - ACCELEROMETER

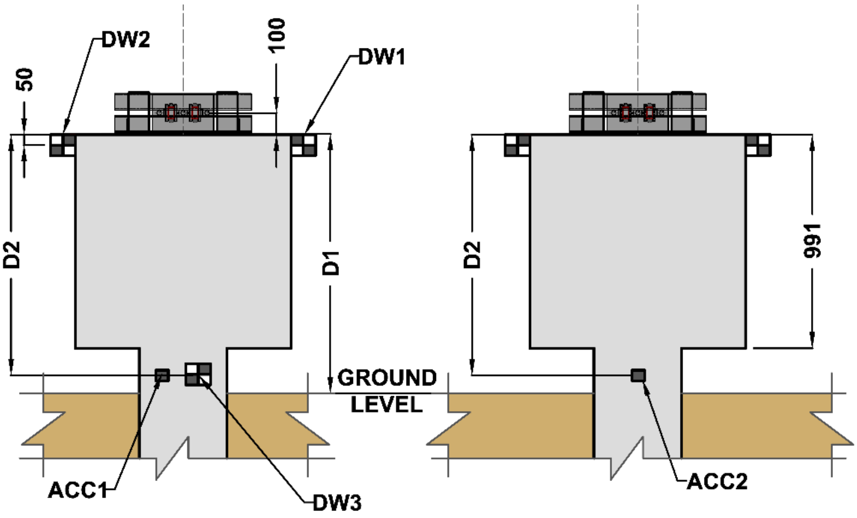

(a) (b)

Figure A9: Locations of instruments on the test pile: (a) South face; (b) North face.

Testing Sequence

To understand the influence of loading sequence on the response of the test piles, a range of different static cyclic loading protocols presented in Table A-1 were used. A single cyclic test was performed to characterise the monotonic response in the first loading direction, and the influence of large displacement on the response in the opposite direction. The target displacements for Pile 1 and Pile 4, measured relative to the initial location of the pile, are summarised in Table A-1. One of the characteristics identified from the monotonic response was the point where significant softening of the pile-soil system started, considered as the yield point in the context of this testing. As discussed in subsequent sections, a yield point of 60 kN was used to inform the development of the multi-cycle loading protocols in Table A-1. For these protocols, the cycles below the yield point were force controlled and the cycles beyond the yield point were displacement controlled. Both Pile 2 and Pile 5 were subjected to increasing cyclic loading to characterise the cyclic response of a typical pile at each pier. Pile 3 was loaded up to the yield point in its first cycle and then tested under increasing cyclic loading (similar to Pile 2), to assess the effect of higher initial loading on the response of the pile. Pile 6 was tested with large post-yield point displacements and was loaded twice at each target displacement level to understand the effect of repeated loading.

Table A-1: Target peak load/displacement values at the end of cycle at the top of pile.

Cycle	Pier 77			Pier 79		
	Pile 1	Pile 2	Pile 3	Pile 4	Pile 5	Pile 6
1	250 mm	20 kN	60 kN	300 mm	20 kN	50 mm
2	-	40 kN	20 kN	-	40 kN	50 mm
3	-	60 kN	40 kN	-	60 kN	100 mm
4	-	50 mm	60kN	-	50 mm	100 mm
5	-	100 mm	50 mm	-	100 mm	150 mm
6	-	150 mm	100 mm	-	150 mm	150 mm
7	-	-	150 mm	-	-	-

Appendix B Experimental Results

The field-testing observations from all the single cycle and multi-cycle pushover tests of the isolated piles are discussed in this section. The results are presented in terms of the load-displacement response at the top of the pile cap using the average of the displacements from both the draw-wires at the top of the pile. In all the load-displacement plots, the displacements and loads corresponding to northern loading direction were shown on the positive axes.

1.1.1. Single Cycle Pushover Testing

The load-displacement response at the top of the pile cap for the single cycle pushover testing of Pile 1 is presented in Figure B1, and the load-displacement response for Pile 4 is presented in Figure B2.

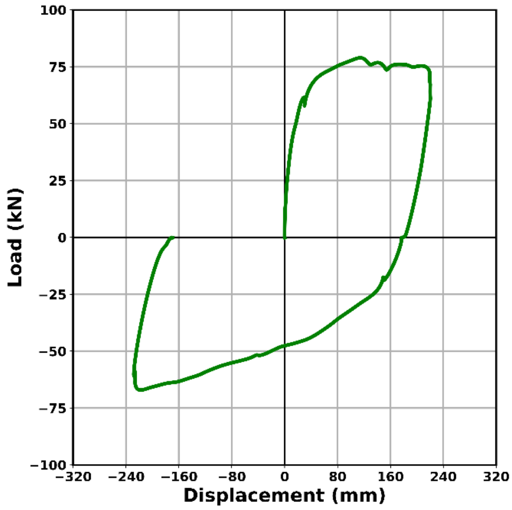

Figure B1: Load-displacement measured at the top of the pile cap in Pile 1

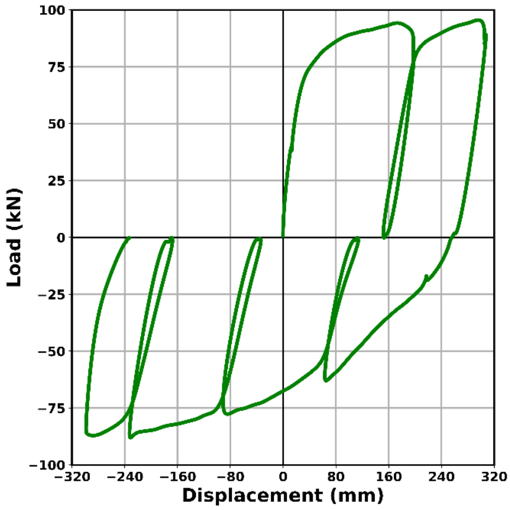

Figure B2: Load-displacement measured at the top of the pile cap in Pile 4

For both Pile 1 and Pile 4, the stiffness of the pile-soil system during unloading and reloading was similar to the initial stiffness of the pile-soil system until the soil gap was closed (Figure B3). The reloading path and the amount of residual displacement, when unloaded and loaded in the southern direction, were identical between Pile 1 and Pile 4. This response suggests that the pile cross-sectional characteristics was dominating the response of the pile-soil system in these ranges.

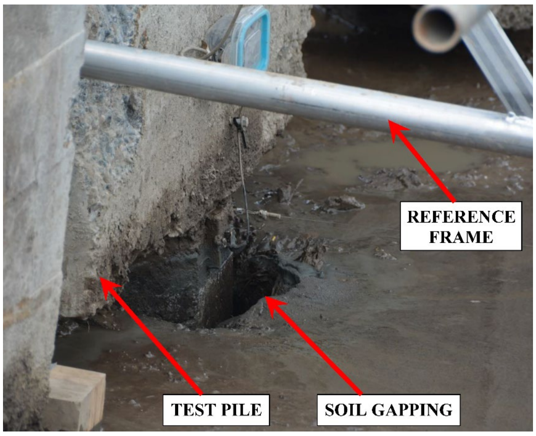

Figure B3: Soil gapping observed around test pile at ground level during testing.

Multi-Cycle Pushover Testing

The pile response from Pile 1 and Pile 4 were used to inform the development of the loading protocols of multi-cycle pushover testing of the piles within each respective pile groups. The response of Pile 1 was used to inform the protocol for Pile 2 and Pile 3, and the response of Pile 4 was used to inform the protocol for Pile 5 and Pile 6.

Increasing Cyclic Loading

The cyclic load-displacement response at the top of Pile 2 subjected to increasing cyclic loading is presented in Figure B4 and the load-displacement response of Pile 5 with the same loading protocol is shown in Figure B5.

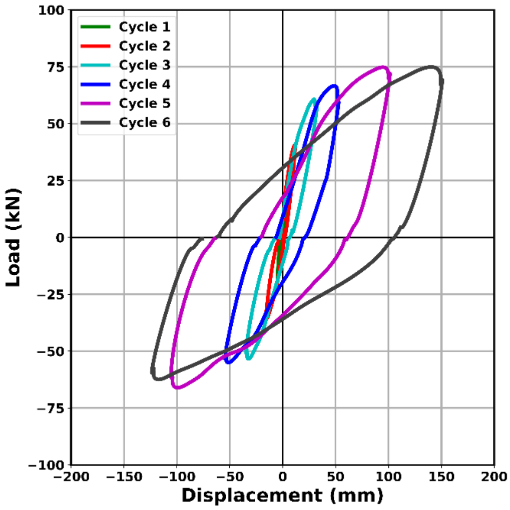

Figure B4: Load-displacement measured at the top of pile cap in Pile 2.

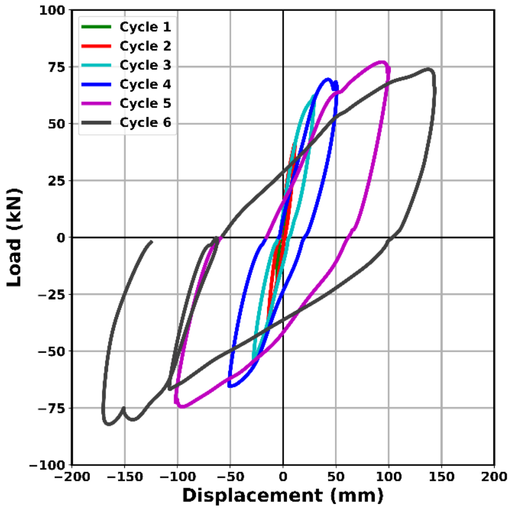

Figure B5: Load-displacement measured at the top of pile cap in Pile 5.

Initial Pre-Yield Load Cycle Followed by Increasing Cyclic Loading

Pile 3 was subjected to an initial cycle that was slightly less than the yield point load and then repeated the loading protocol used by Piles 2 and 5 in order to study the effects of initial soil gapping and non-linearity on the cyclic response. The cyclic load-displacement response at the top of the pile from the testing of Pile 3 is presented in Figure B6.

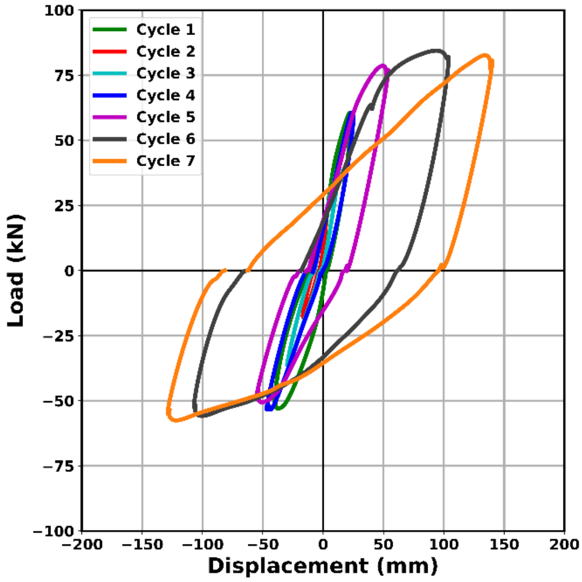

Figure B6: Load-displacement measured at the top of pile cap in Pile 3.

Repeated Loading Cycles

Pile 6 was subjected to large post-yield point displacements and was loaded twice at each target displacement level. The cyclic load-displacement response at the top of pile from the testing of Pile 6 is presented in Figure B7.

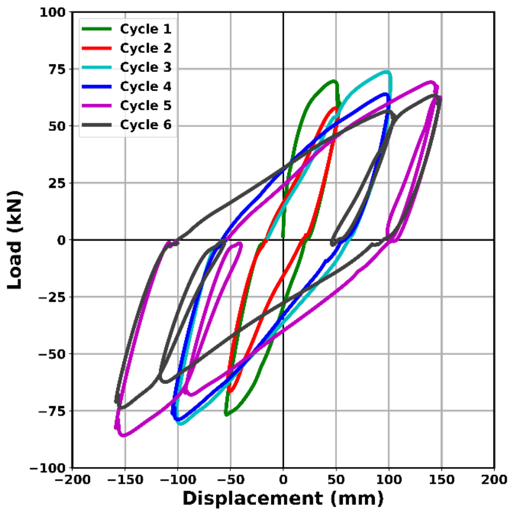

Figure B7: Load-displacement measured at the top of pile cap in Pile 6

Appendix C Pile Model

Model development

Finite element models (FEM) of the test piles discussed in the previous section were developed based on a Nonlinear Beam on Winkler Foundation approach using the open-source analysis software OpenSeesPy (Zhu et al., 2018). The models were developed to replicate the lateral response of reinforced concrete bridge pile foundations with smooth reinforcement under various loading conditions whilst accounting for material nonlinearity and the influence of the smooth reinforcement.

Model Overview

A schematic representation of the pile-soil system is presented in Figure C1. The pile elements were modelled using displacement based distributed plasticity beam-column elements with three integration points per element, with a convergence study undertaken to determine the number of elements required to adequately capture the response in terms of both pile and soil response. The pile cap was discretised into 5 equal length elements while the pile was divided into 47 elements, with smaller elements in the top 4 m to capture the behaviour in the active pile length region (Davies and Budhu, 1986). No P-delta effects were considered when modelling these experiments, as there was no additional axial load applied to the piles during testing.

Displacement controlled lateral loading histories were applied to the top of the specimen using the displacement histories recorded during the experiments. All loading cycles were modelled sequentially in order to capture any of the residual deformations that developed. The maximum displacement applied at the end of each loading cycle were equal to the values summarised in Table C1.

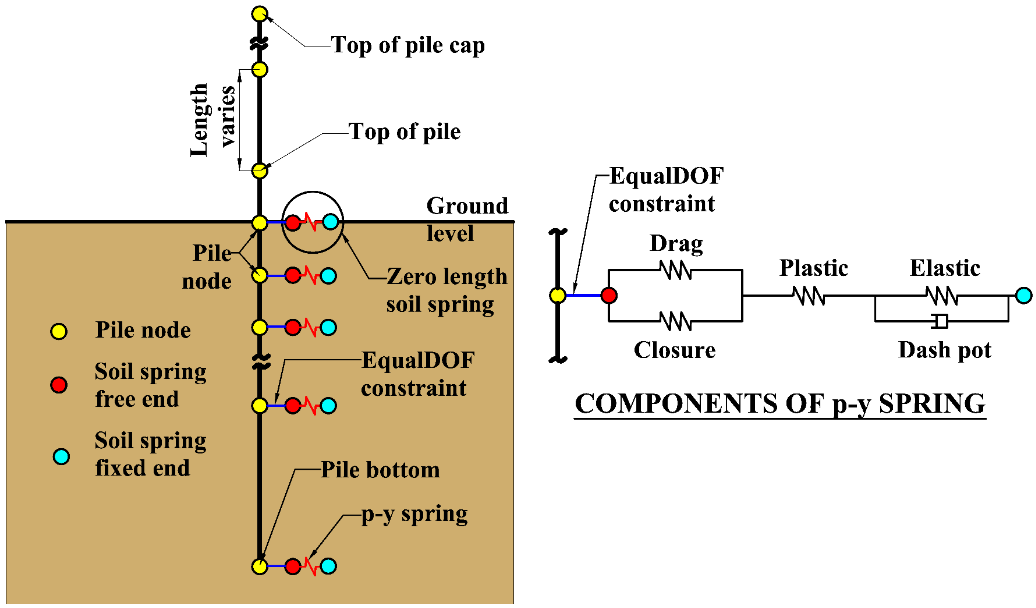

Figure C1: OpenSeepy model representation of pile-soil interaction, displacement based beam-column elements and fibre section.

Pile-Column Modelling

The nonlinear behaviour of the pile-column was modelled using a fibre-based approach with cross-sectional characteristics summarised in Figure C1. The core concrete was divided into 30 radial divisions and into 36 circumferential divisions, with the cover concrete divided into 10 radial division and 36 circumferential divisions.

Unconfined and confined concrete fibres were modelled using the Kent-Scott-Park material model with linear tension stiffening (Concrete02 in OpenSeesPy). The properties for each concrete material model are summarised in Table C1 with confined concrete properties defined using the Mander et al. (1988) model. The characteristic concrete strength (f'_c) used in the numerical models was determined based on compressive strength tests performed in the laboratory on core samples collected on site, and concrete tensile strengths (f_{ct}) were defined using Standards New Zealand (2006) guidance. Steel reinforcement fibres were modelled using a Giuffré-Menegotto-Pinto formulation implemented by Menegotto and Pinto (Steel02 in OpenSeespy) with a yield strength of 280 MPa based on recommendations from Maffei (1996). A rupture strain of 20% (Andriono and Park, 1986) was applied using the "MinMax" material in OpenSeespy.

Table C1: Material properties used in the OpenSeesPy model for confined and unconfined concrete.

Region	f'c (MPa)	Peak strain	Tensile strength (MPa)
Unconfined	40.0	0.0028	4.2
Confined	45.2	0.0046	4.2

Bond-Slip Modelling

Fibre sections in OpenSees follow the assumption that plane sections remain plane, meaning perfect bond is assumed between the steel reinforcement and surrounding concrete. To account for the influence of bond slip on the stress-strain response of smooth reinforcement, a modified bilinear steel reinforcement material model was used. The original material model is shown in Figure C2 and is based on initial stiffness (E), strain hardening ratio (b), steel yield strain (ε_{sy}), and ultimate steel strain (ε_{su}) parameters. The modified version of this material model is referred to as the bond-slip material model herein. The bond-slip material model is shown in Figure C2 with a reduced initial stiffness (E'), a modified value of steel yield strain (ε'_{sy}), and a modified value of ultimate steel strain (ε'_{su}). The yield (f_y), the strain hardening ratio (b), and rupture stress (f_u) values remain unchanged in this approach. The process of determining these changes is discussed below in this section.

As there are no readily available bond-slip material models for plain round bars that can be implemented using the distributed bond slip modelling approach, the bond-slip material model parameters were estimated based on the procedures developed by Dehestani and Mousavi (2015) for deformed bars. A detailed overview of this methodology is described in Evangelio (2021). The final bond-slip material model parameters used for the Whirokino Trestle Bridge piles were calculated to be E' of 125 GPa and ε'_{su} of 0.236 per the recommendations in Dehstani and Mousavi (2015).

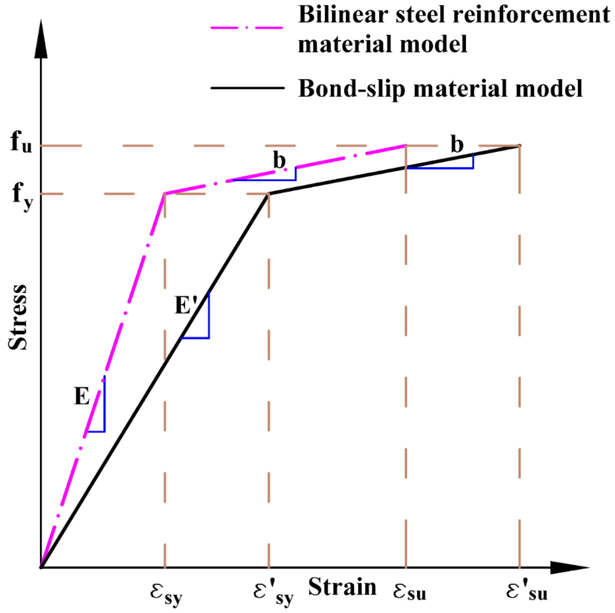

Figure C2: Comparison of original constitutive relationship and the modified (including bond-slip effects) constitutive relationship for steel material

Soil Modelling

Soil was modelled using nonlinear p-y springs in OpenSeesPy (Boulanger, 1999) and implemented using zero length elements with cyclic load-displacement relationships. The non-linear behaviour of the p-y spring was modelled using elastic, plastic and gap components in series and can be seen in Figure C1. The gap component consists of a non-linear closure spring in parallel with non-linear drag spring, to represent soil drag along the side of the pile. The CPT tip resistance (q_c) was used to define the friction angle and soil unit weight for each of the soil layers based on the correlations of Robertson (2010). The average friction angle and soil unit weight for each layer were used to define the ultimate capacity of the p-y springs (p_{ult}) and the displacement at which 50% of p_{ult} was mobilised (y_{50}) within that layer based on the recommendations from API (1987) for sand. As the loading was applied in the lateral direction only, no t-z or q-z springs were included in the model.